Study on water column impact without/with air cavity

Bingyue Song[1], Chongwei Zhang[2]

1. Department of Electric Power Engineering, Kunming University of Science and Technology, Kunming 650504, China
2. State Key Laboratory of Coastal and Offshore Engineering, Dalian University of Technology, Dalian 116023, China
Email: bingyue_song@163.com; chongweizhang@dlut.edu.cn

1 Introduction

Three-dimensional plunging wave impact enclosing an air cavity under the free surface is a very complex phenomenon in coastal engineering. To help understanding some physics behind it, this paper studies a simplified impact model of axisymmetric water column without/with air entrapment. Potential-flow theory that assumes the fluid to be inviscid, incompressible and flow-irrational is used. The air entrapped in the water front is assumed to abide the adiabatic law. Both analytical and numerical investigations are carried out.

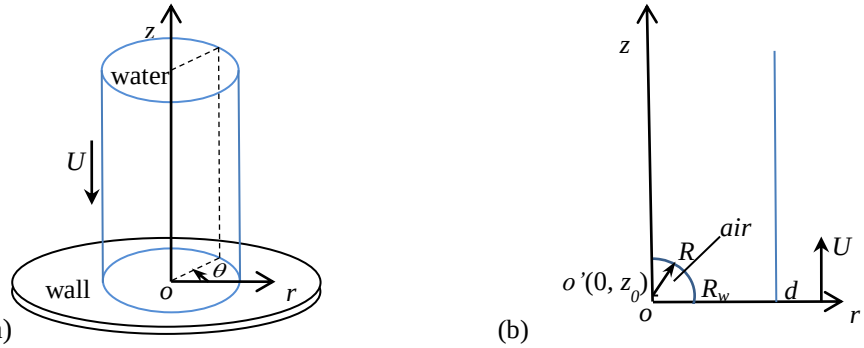

Figure 1. (a) Stretch of the problem; (b) projection of the initial impact at any azimuth, with a spherical air cavity centred at (0, z_0)

Consider a cylindrical liquid column of radius d hitting a rigid wall with a constant velocity U, as shown in Fig. 1(a). This is dynamically equivalent to the case where the water column is at rest and the rigid wall moves against it. A cylindrical coordinate system $o-r\theta z$ is established. The 3D problem can then be solved in a plane coordinate system o-rz, as shown in Fig. 1(b). A spherical air cavity of radius R is entrapped with its centre located at (0, z_0). It intersects on the wall with radius R_w. The boundary value problem (BVP) of the velocity potential ϕ can be written as

$$\nabla^2\phi = 0, \text{ in the fluid domain} \tag{1}$$

$$\phi = 0, \text{ on the free surfaces for } t = 0 \tag{2}$$

$$\frac{\partial\phi}{\partial n} = -U, \text{ at } z = 0 \tag{3}$$

$$\frac{\partial\phi}{\partial n} = 0, \text{ at } z \to \infty \text{ and along } r = 0 \tag{4}$$

The pressure can be obtained after solving the BVP of ϕ_t. The variable of ϕ_t satisfies Laplace's equation and the following boundary conditions

$$\phi_t = -\frac{1}{2}\nabla\phi\cdot\nabla\phi, \text{ on the outer free surface} \tag{5}$$

$$\phi_t = -\frac{1}{2}\nabla\phi\cdot\nabla\phi - \frac{P_a}{\rho}\left[\left(\frac{V_0}{V}\right)^{\gamma} - 1\right], \text{ on the cavity surface} \tag{6}$$

$$\frac{\partial\phi_t}{\partial n} = -\vec{u}\cdot\frac{\partial\nabla\phi}{\partial n}, \text{ at } z = 0 \quad \text{(Wu 1998)} \tag{7}$$

$$\phi_t = 0, \text{ at } z \to \infty \tag{8}$$

where P_a is the atmospheric pressure, ρ is the density of water, $\gamma = 1.4$ is the heat radio of the air, V is the volume of entrapped air, and V_0 is the initial value of V. The above BVPs can be solved by the boundary element method (BEM) in the time domain. A shallow water approximation of $\phi = A + B\ln r + Cz$ is specially applied in the thin jet region for numerical efficiency and accuracy.

2 Some analytical deductions

2.1 On the initial instant

Using the method of separation of variables, the solution of Laplace's equation in the cylindrical coordinate system has the following form

$$\phi = \sum_{n=0}^{\infty} A_n e^{-\lambda_n z} J_0(\lambda_n r) \tag{9}$$

where $J_0(x)$ is the zeroth order Bessel function (Abramowitz & Stegun 1972), and A_n and λ_n are corresponding parameters. According to boundary conditions in Eqs. (2)-(4), the solution can be written as

$$\phi(r,z) = -2Ud\sum_{n=0}^{\infty}\frac{1}{\mu_n^{\,2}J_1(\mu_n)}e^{-\mu_n\frac{z}{d}}J_0(\mu_n\frac{r}{d}) \tag{10}$$

where $J_1(x)$ is the first order Bessel function, and μ_n denotes the n*th* root of $J_0(x)=0$. From Bernoulli's equation, the pressure impulse at the impact instant $\Pi=\int_{0_-}^{0_+}pdt=\int_{0_-}^{0_+}-\rho\phi_t dt=-\rho\phi$ (Batchelor 1967, p.471) follows that of the initial potential, from 0 at the free surface *r*=*d* to a maximum value at the impact centre *r*=0 along the wall. Nevertheless, Wu (2001) solved the initial impact pressure by a 2D rectangular water column and found it to be a constant value of ρU^2, before dropping abruptly to 0 at the intersection. We may speculate whether there are similar features in the present axisymmetric problem. Substituing Eq. (10) into Eqs. (5), (7) & (8), the solution of ϕ_t is found to take the form

$$\phi_t = -U\phi_z - 2U^2\sum_{n_1=0}^{\infty}\sum_{n_2=0}^{\infty}\frac{J_0[(\mu_{n_1}^{(0)}+\mu_{n_2}^{(0)})\frac{r}{d}]e^{-(\mu_{n_1}^{(0)}+\mu_{n_2}^{(0)})\frac{z}{d}}}{\mu_{n_1}^{(0)}\mu_{n_2}^{(0)}J_0(\mu_{n_1}^{(0)}+\mu_{n_2}^{(0)})}+\sum_{n=0}^{\infty}a_nJ_0(\mu_n^{(0)}\frac{r}{d})e^{-\mu_n^{(0)}\frac{z}{d}} \tag{11}$$

where $a_n=\frac{4U^2}{\mu_n^{(0)}d^2J_1^2(\mu_n^{(0)})}\int_0^d rJ_0(\mu_n^{(0)}\frac{r}{d})\sum_{n_1=0}^{\infty}\sum_{n_2=0}^{\infty}\frac{(\mu_{n_1}^{(0)}+\mu_{n_2}^{(0)})}{\mu_{n_1}^{(0)}\mu_{n_2}^{(0)}J_0(\mu_{n_1}^{(0)}+\mu_{n_2}^{(0)})}J_0[(\mu_{n_1}^{(0)}+\mu_{n_2}^{(0)})\frac{r}{d}]dr$. However, the result of the series is found failing to converge at *z*=0 in the present form, which demands further investigation.

2.2 On the steady state

For the case of water column impact with unit radius and velocity, Bernoulli's equation and the kinetic condition are satisfied on the free surface $z=\varsigma(r,t)$

$$\frac{\partial\phi}{\partial t}+\frac{1}{2}\left[\left(\frac{\partial\phi}{\partial r}\right)^2+\left(\frac{\partial\phi}{\partial z}\right)^2\right]=\frac{1}{2} \tag{12}$$

$$\frac{\partial\phi}{\partial r}\varsigma_r-\frac{\partial\phi}{\partial z}=\varsigma_t \tag{13}$$

At the steady state, the combination of Eqs. (12)&(13) leads to

$$\frac{\partial\phi}{\partial r}=\frac{1}{\sqrt{1+\varsigma_r^2}},\quad \frac{\partial\phi}{\partial z}=-\frac{1}{\sqrt{1+1/\varsigma_r^2}} \tag{14}$$

Eq. (14) shows that ϕ_r approaches 1 as $\varsigma_r\to 0$ on the free surface at the steady state. Further consider the conservation law of mass

$$\int_0^{\varsigma}2\pi r\frac{\partial\phi(r,z)}{\partial r}dz=\pi \tag{15}$$

and Taylor's expansion for ϕ_r with respect to *z*, we can find the steady state satisfying

$$\frac{\varsigma}{\sqrt{1+\varsigma_r^2}}-\frac{1}{2r}+O(\varsigma^3)=0 \tag{16}$$

3 Results & discussions

3.1 Impact by pure water

The initial column radius *d*, water density ρ and impact velocity *U* are utilized for nondimensionalisation. Fig. 2 illustrates the evolution of local free surface profiles and pressure variation along the wall at any azimuth. Right after the initial impact instant at $t=0_+$, the pressure is found to increase gradually from around 0.8 at the impact centre to around 1 at the intersection, and then drops sharply to the zero ambient pressure. After the initial impulsive stage, a thin jet begins to form along the wall. Meanwhile, the pressure starts to fall slowly from the impact centre to the jet root. As the impact continues, the overall impact dynamics vary more and more slowly along the wall.

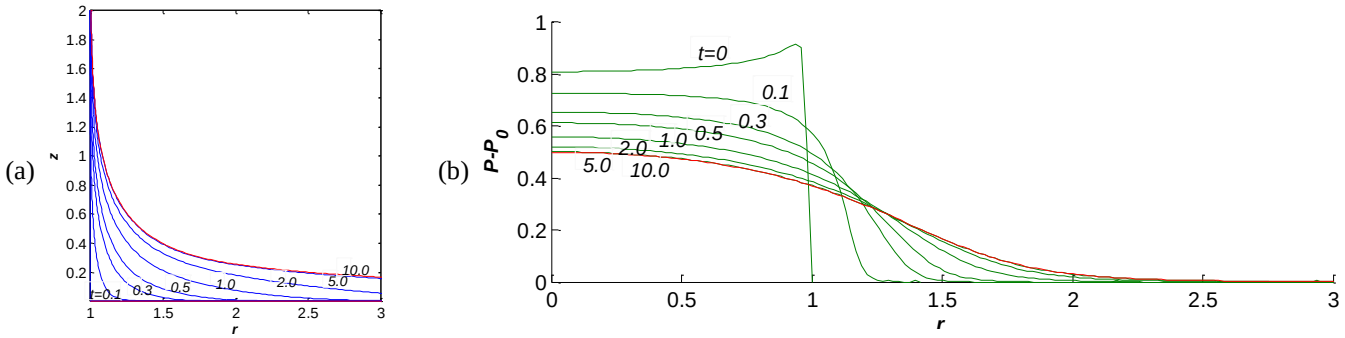

Figure 2. Snapshots of water column impact on the wall: (a) free surface deformation and (b) pressure variation along the wall

From the variation of ϕ_r along the free surface shown in Fig. 3, we can see that continuously increasing span of the flow is reaching the steady state in the time domain, according to Eq. (14). Fig. 4 shows temporal histories of the total force and pressure at the stagnation point (0,0). The former is found to approach 1, equal to the changing rate of flow momentum in the *z*-axis direction. The latter is found to decrease from around 0.8 to 0.5, satisfying Bernoulli's equation for a steady flow. The steady state shown here corresponds to that of the main fluid domain in spite of the stretching thin jet. The steady-state solution may also refer to the self-similar solution of impact by a water cone with its inner angle approaching zero in Sun & Wu (2014).

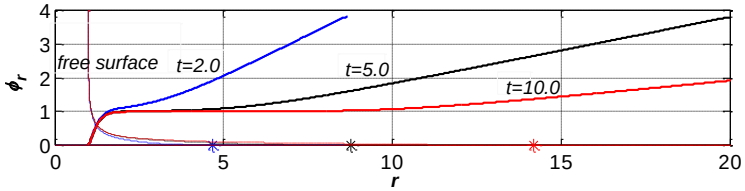

Figure 3. Variation of ϕ_r along the free surface (the asterisk denotes the starting point of shallow water approximation)

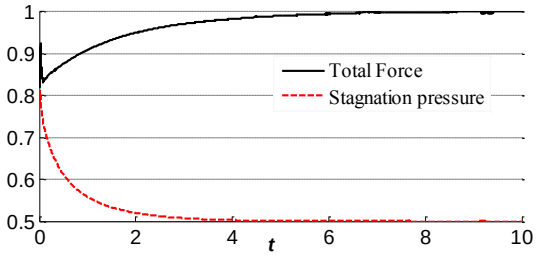

Figure 4. Histories of the total force and stagnation pressure

3.2 Air cavity effect

The entrapped air would inevitably affect the initial impact pressure. However at this stage the result is still immune to the value of initial air pressure P_0 and only affected by its size and shape/thickness. From Figs. 5&6, it can be seen that the entrapment of an air cavity can significantly increase the initial impact pressure. Besides, cavity with smaller size on the wall and thinner shape (i.e. z_0<0 in Fig. 1(b)) can lead to a larger pressure maximum, located near the cavity-wall intersection.

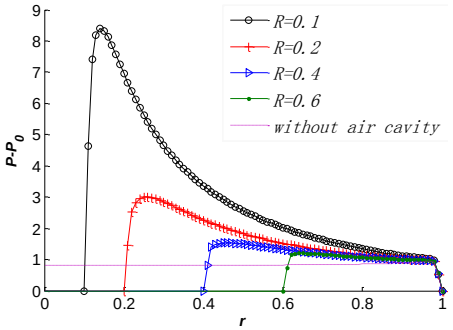

Figure 5. Initial impact pressure with different sizes of hemispherical cavity (i.e. z_0=0)

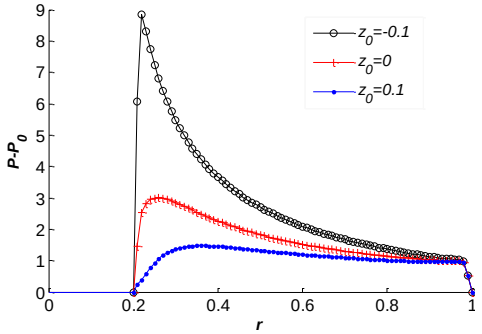

Figure 6. Initial impact pressure with different cavity shapes/thickness: z_0=-0.1, 0 and 0.1 for thin to thick ones (R_w=0.2)

To give an intuitive description of the effect of the entrapped air, the subsequent impact process with hemispherical cavity (z_0 =0) of R=R_w=0.2 is shown in Fig. 7. The initial air pressure is set to be P_0=100, corresponding to an impact velocity of U=0.9934m/s. The entrapped air is initially compressed by the impacting flow (see Fig. 7(a)), and then starts to expand after it reaches the minimum volume at t=0.012 (see Fig. 7(b)). Pressure on the wall oscillates accordingly, which becomes negative after t=0.0239. The radial jet impinges at the impact centre at t=0.0295. After that a vertical jet starts to shoots up with an average velocity exceeding 70, as shown in Fig. 7(c). At early stage of the formation of the vertical jet, a pressure spike appears at its bottom, to provide the large acceleration for the local fluid particles there (see at t=0.030). The jet reaches the top cavity surface at t=0.0326. After that a ring cavity is expected to be formed, which is not included in the current study. Applying the conservation law of energy at the moment when the air cavity is compressed to its minimum volume and reaches the maximum pressure P_{max}, we have (see also in Bredmose et al. (2015), Song & Zhang (2018))

$$\left(\frac{P_{\max}}{P_0}\right)^{\frac{\gamma-1}{\gamma}}+(\gamma-1)\left(\frac{P_{\max}}{P_0}\right)^{-\frac{1}{\gamma}}-\gamma=-\frac{\delta K}{E_{a0}} \tag{17}$$

where δK is the increment in the kinetic energy of the water, and $E_{a0}=P_0V_0/(\gamma-1)$ is the defined potential energy of the air.

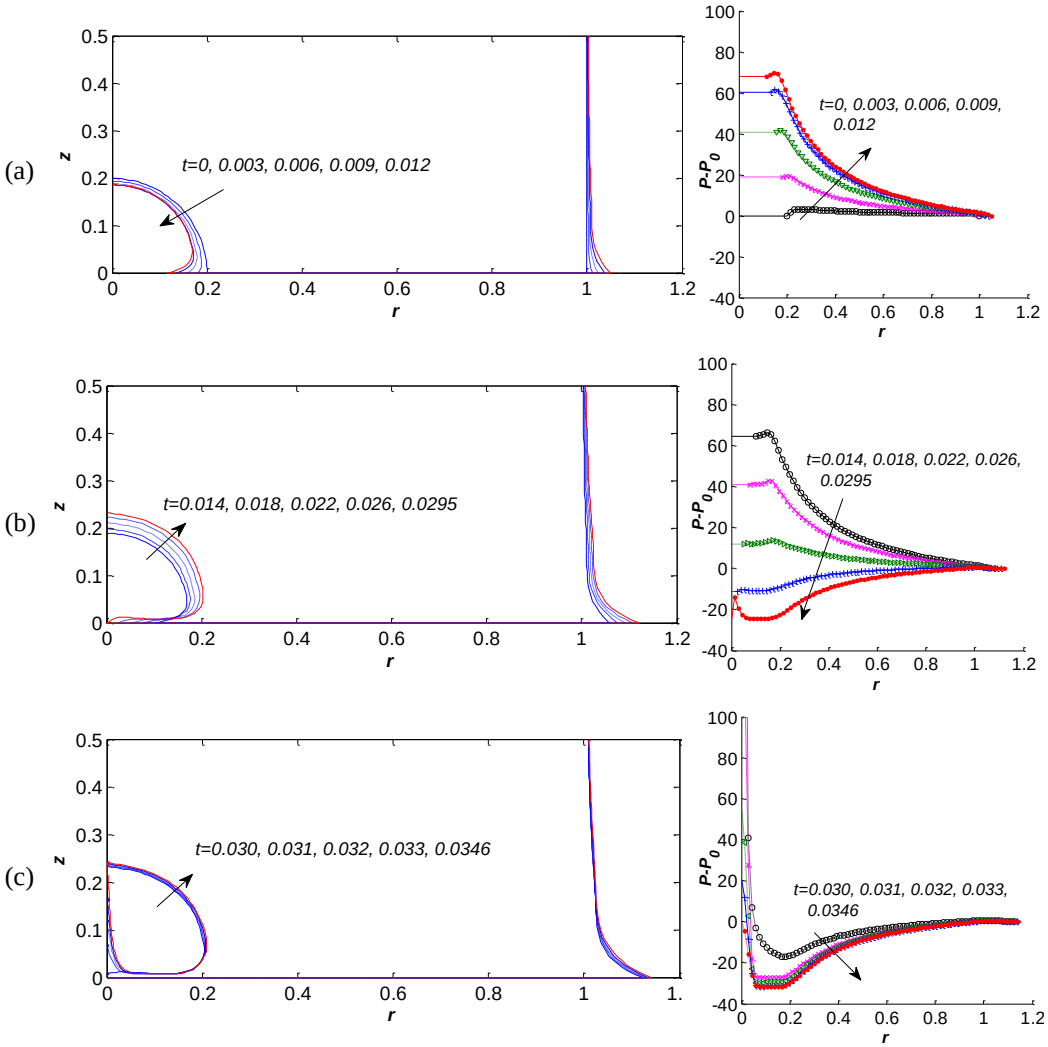

Figure 7. Water column impact with a hemispherical cavity entrapped (case 1- z_0 =0, R=R_w=0.2, P_0 =100): deformation of the free surface (left) and the corresponding impact pressure (right): (a) contraction stage; (b) expansion stage i: formation of radial jet along the wall until impingement; (c) expansion stage ii: formation of the vertical jet

More case studies of impact with various cavity shape/thickness (z_0), size V_0 and initial pressure P_0 will be presented in the workshop, along with quantitative analysis on the effect of V_0 and P_0 on P_{max} based on Eq. (17).

Acknowledgement

We would like to acknowledge the financial support by the National Natural Science Foundation of China (No. 51709038, 51669008 & 51569011), the Project funded by China Postdoctoral Science Foundation (No. 2018M630289), Open Fund of the State Key Laboratory of Coastal and Offshore Engineering (No. LP1820) and Natural Science Foundation of Kunming University of Science and Technology (No. KKSY201604033). The authors are grateful to Prof G. X. Wu from University College London for the helpful discussions on this work.

References

[1] Wu G.X., 1998. Hydrodynamic force on a rigid body during impact with liquid. J Fluid Struct 12, 549-559.
[2] Abramowitz M., Stegun I.A., 1972. Handbook of Mathematical Functions With Formulas, Graphs and Mathematical Tables. Washington D.C.
[3] Batchelor G.K., 1967. An Introduction to Fluid Mechanics. Cambridge: Cambridge University Press.
[4] Wu G.X., 2001. Initial pressure distribution due to jet impact on a rigid body. J Fluid Struct 15, 365–370.
[5] Sun S.L., Wu G.X., 2014. Self-similar solution for oblique impact of a water column with sharp front on a wall and its zero inner angle steady limit. Phys. Fluid 26, 082106.
[6] Bredmose H., Bullock G.N., Hogg A.J., 2015. Violent breaking wave impacts. Part 3: effects of scale and aeration. J Fluid Mech 765, 82–113.
[7] Song B., Zhang C., 2018. Boundary element study of wave impact on a vertical wall with air entrapment. Eng Anal Boundary Elem 90, 26-38.